Hygroscopic properties of potassium-halide nanoparticles

Giamarelou, M; Smith, M.; Papapanagiotou, E.; Martin, S. T.; Biskos, G.

DOI
10.1080/02786826.2018.1432848

Publication date
2018

Document Version
Final published version

Published in
Aerosol Science and Technology

Aerosol Science and Technology

ISSN: 0278-6826 (Print) 1521-7388 (Online) Journal homepage: http://www.tandfonline.com/loi/uast20

Hygroscopic properties of potassium-halide nanoparticles

M. Giamarelou, M. Smith, E. Papapanagiotou, S.T. Martin & G. Biskos

To cite this article: M. Giamarelou, M. Smith, E. Papapanagiotou, S.T. Martin & G. Biskos (2018): Hygroscopic properties of potassium-halide nanoparticles, Aerosol Science and Technology, DOI: 10.1080/02786826.2018.1432848

To link to this article: https://doi.org/10.1080/02786826.2018.1432848

AEROSOL SCIENCE AND TECHNOLOGY
https://doi.org/10.1080/02786826.2018.1432848

Hygroscopic properties of potassium-halide nanoparticles

M. Giamarelou[a], M. Smith[b], E. Papapanagiotou[a], S.T. Martin[b], and G. Biskos [c,d]

[a]Department of Environment, University of the Aegean, Mytilene, Greece; [b]School of Engineering and Applied Sciences, Harvard University, Cambridge, Massachusetts, USA; [c]Faculty of Civil Engineering and Geosciences, Delft University of Technology, Delft, The Netherlands; [d]Energy Environment and Water Research Center, The Cyprus Institute, Nicosia, Cyprus

ABSTRACT

The hygroscopic properties of KBr, KCl, and KI nanoparticles having diameters from 8 to 60 nm were measured using a tandem Differential Mobility Analyzer. In all cases, the deliquescence and efflorescence relative humidity values increased with decreasing particle diameter. The associated growth factors also decreased with decreasing particle diameter, in agreement with predictions by Köhler theory. Overall, the theoretically predicted growth factors agreed well with the measurements, i.e., within ±3% uncertainty. For KCl particles having sizes down to 15 nm, however, a dynamic shape factor of 1.08, corresponding to non-spherical crystalline particles prior deliquescence, was inferred for agreement between measurements and theory. By comparison, KBr and KI within the same size range warranted shape factors of unity, equivalent to a sphere. These results contribute to an understanding of nanosize behavior widely relevant to material sciences as well as atmospheric aerosol particles over the oceans.

ARTICLE HISTORY
Received 24 July 2017
Accepted 3 January 2018

EDITOR
Ilona Riipinen

1. Introduction

Inorganic salt particles suspended in the atmosphere can exist in either the solid or the aqueous-solution state depending on whether they have been exposed to low or high relative humidity (RH) conditions (Tang and Munkelwitz 1994; Martin 2000; Wise et al. 2005). The points in RH space where the transition from solids to aqueous solutions take place (i.e., the deliquescence RH; DRH) or vice versa (i.e., the efflorescence RH; ERH) can differ substantially, leading to a hysteresis effect (Martin 2000; Topping 2008; Biskos et al. 2006a; Mifflin et al. 2009). At RH values between DRH and ERH, the particles can be either solid or aqueous depending on their RH history (Wexler and Seinfeld 1991). In the aqueous state, the water content of the particles can be predicted by Köhler theory (Köhler 1936), which takes into account the water vapor pressure reduction over a concentrated solution droplet (i.e., Raoult's law) and the water vapor pressure increase due to high curvature of the droplet (i.e., the Kelvin effect). As a result of the Kelvin effect, the water uptake of the aqueous droplets is reduced as particle size decreases below 50 nm (Köhler 1936; Seinfeld and Pandis 2006; Pruppacher and Klett 1997), which in turn affects the size of the resulting droplets.

Since the pioneering work of Köhler (Köhler 1936) in the 1930's, many studies have investigated the hygroscopic behavior of pure inorganic aerosol particles having diameters greater than 100 nm using electrodynamic balances (Tang and Munkelwitz 1977; 1993; Zhang and Chan 2002; Tang et al. 1997) and mobility analysis (Tang et al. 1997; Tang and Munkelwitz 1977; Tang 1996). Particles in the nanosize regime (i.e., particles having diameters <100 nm) can exhibit altered physical properties compared to larger particles (Anastasio and Martin 2001). For RH < DRH, the Gibbs free energy of the crystalline salt particles is lower than that of the aqueous-vapor system (Seinfeld and Pandis 2006), and thus the particles remain solid. Deliquescence is a thermodynamically driven process that occurs at the RH corresponding to the solubility of the salt. When crystalline

CONTACT S.T. Martin smartin@seas.harvard.edu School of Engineering and Applied Sciences, Harvard University, Pierce Hall 122, 29 Oxford St., Cambridge, MA 02138, USA; G. Biskos g.biskos@cyi.ac.cy Energy Environment and Water Research Centre, The Cyprus Institute, Nicosia 2121, Cyprus; or Faculty of Civil Engineering and Geosciences, Delft University of Technology, Delft, 2628, The Netherlands.

Color versions of one or more of the figures in the article can be found online at www.tandfonline.com/uast.

Supplementary files for this article can be accessed on the publisher's website.

inorganic salt particles are exposed to RH ≥ DRH, they spontaneously take up water to form aqueous droplets and thus promptly increase their diameter.

Experiments have been designed to study these effects in the nanosize regime. The DRH of sub-50-nm NaCl particles, for example, was shown to increase with decreasing particle size as a result of the higher contribution of surface energy to the total free energy of the gas-particle system (Biskos et al. 2006a). Rather than thermodynamics, the efflorescence of aqueous salts is the result of homogeneous nucleation (Seinfeld and Pandis 2006). The nucleation rate is inversely proportional to the concentration of ions in the droplet and thus scales to the third power of its size (i.e., to its volume). As a result of the Kelvin effect, the required RH for maintaining a small enough droplet within which nucleation of the soluble species can initiate (i.e., the ERH) increases when size decreases below approximately 50 nm (Martin 2000; Gao et al. 2006; 2007; Hameri et al. 2000). This understanding, however, remains in need of theory development because even as NaCl particles follow this behaviour (Biskos et al. 2006a), $(NH_4)_2SO_4$ particles do not (Biskos et al. 2006b). Further observations of other test compounds are needed for greater generalization of the understanding of DRH and ERH behaviour of nano-sized salt particles.

In regard to which systems to prioritize in these additional studies, particles that occur in the atmospheric environment typically are internal mixtures of a number of compounds. Over oceans, for example, sea salt particles consist of Na^+, Mg^{2+}, K^+, Cl^-, SO_4^{2-}, Br^-, and I^- with magnesium and potassium being minor but important components (Seinfeld and Pandis 2006; Kelly and Wexler 2006). Potassium compounds are also associated with biomass burning aerosols (Liu et al. 2000). The hygroscopic properties of common atmospheric nanoparticles (i.e., NaCl and $(NH_4)_2SO_4$) having diameters smaller than 50 nm have systematically been studied by Hameri et al. (2000; 2001) and later by Biskos et al. (2006a,b,c) and Gao et al. (2006, 2007). Pure letovicite particles as well as mixtures of letovicite and ammonium bisulfate, having diameters ranging from 15 to 60 nm have also been studied by Mifflin et al. (2009). Herein, we report new measurements of the DRH, ERH, and hygroscopic growth factors of potassium-halide particles (namely, KBr, KCl, and KI) having diameters from 8 to 60 nm. The findings fill a missing gap in the literature and expand the existing knowledge on the hygroscopic behavior of inorganic salt nanoparticles, thereby helping us understand their role in the atmosphere.

2. Methodology

2.1. Experimental

2.1.1. Generation of aerosol particles

The vaporization-condensation technique was used to generate all the salt nanoparticles for the needs of this study. The advantage of this technique is that it generates particles of very high purity (Biskos et al. 2006a,c; Scheibel and Porstendorfer 1983), in part because no solvent is required. To synthesize the particles, high-purity (>99.5%) granular salts were placed within a quartz tube inserted in a Thermolyne (Model 21100) tube furnace. Ultrapure N_2 was passed continuously through the tube, which was maintained at high temperatures. Salt vapors produced by the high temperatures were carried by the N_2 flow downstream the furnace where they were cooled down to room temperature thereby forming nanoparticles by nucleation. By adjusting the temperature of the furnace from 500 to 700°C, we could produce polydisperse aerosol particles having mean diameters that varied from ca. 10 to 45 nm.

Particles produced by vaporization-condensation are typically highly agglomerated (Flagan and Lunden 1995). A pre-conditioning stage was therefore used to restructure the agglomerates into compact particles before measuring their hygroscopic behavior (Martin 2000; Biskos et al. 2006a,c; Scheibel and Porstendorfer 1983; Flagan and Lunden 1995). To do so, the dry aerosol (RH < 5%) exiting the tube furnace was passed through a Nafion conditioner submerged in water (NCW; Perma Pure Model MD-110) to increase the RH of the aerosol flow above 95%. Subsequently, the RH of the aerosol was decreased to values below 5% by passing it through a Nafion conditioner operated with an RH-adjustable air sheath flow (NCA). The RH history of the conditioned polydisperse aerosol was therefore 5% → 95% → 5%. In all cases, the RH was determined with sensors (Omega Model HX93AV) having an accuracy of ±2.5%.

2.1.2. Measurements of particle hygroscopicity

A tandem nano-differential mobility analyzer (TnDMA) (Rader and McMurry 1986) system was used to investigate the hygroscopic properties of the potassium-halide aerosol particles. Details of the apparatus are provided in Biskos et al. (2006a,c). In brief, the pre-conditioned particles generated by the vaporization-condensation method were passed through a ^{210}Po bipolar charger and a first differential mobility analyzer (DMA-1; TSI 3085). DMA-1, was used to select monodisperse particles, which were then exposed to one of two RH profiles, depending on whether deliquescence- or efflorescence-mode experiments were conducted. For the deliquescence-mode experiments, the RH of the aerosol flowing

downstream of DMA-1 was stepwise increased using an NCA at X% RH before entering a second DMA (DMA-2). The RH history of the monodisperse sample in these experiments was therefore 5% → X%. For the efflorescence-mode experiments, we used an NCW and an NCA in series. The NCW was used to increase the RH of the monodisperse sample downstream of DMA-1 to values >95%, whereas the NCA that followed decreased the RH of the sample in a stepwise manner. The RH history of the monodisperse sample downstream of DMA-1 in this case was 5% → 95% → X%. The mobility distribution of the particles exiting the humidification system was measured by DMA-2 and an ultrafine CPC. The sheath and the aerosol flow in both DMAs were 3 and 0.3 lpm, respectively. In order to ensure that the size of the particles does not change between the RH conditioner and DMA-2, the aerosol flow RH (RH_a) and the sheath flow RH (RH_s) in DMA-2 were continuously measured during the experiments (Biskos et al. 2006b) and their difference was kept <3% (Hameri et al. 2000; Biskos et al. 2006b; Bezantakos et al. 2016). The system was calibrated regularly using 60-nm NaCl particles, which have a well-understood hygroscopic behavior (Biskos 2006c), while the majority of the measurements were conducted two times to ensure consistency.

2.1.3 Data analysis

A modified version of the TDMAfit algorithm (Stolzenburg and McMurry 1988) was used to determine the hygroscopic growth factors of the particles from the hygroscopic TnDMA measurements. The algorithm compensates for differences in the conditions within the experimental setup. More specifically, it corrects the measurements for discrepancies in the measured electrical mobility of the particles by the two DMAs that result from differences in temperature and pressure. The algorithm uses the Levenberg Marquardt least squares algorithm (Marquardt 1963; Markwardt 2010) to fit Gaussian-shaped transfer functions to the measured response of the system. The fitted parameters are (1) the particle penetration through the system, (2) the growth factor of the particles due to their water uptake, and (3) the flow conditions in the two DMAs. To locate the peak positions and the associated particle-number concentrations that give the best fit to the measurements, the algorithm employs a search routine with a number of convergence criteria and constraints. The best solution is reached when a chi-squared function of the fit residual changes by less than 0.1% and each of the fitted parameters deviates by less than 10% of its respective estimated uncertainty (Stolzenburg and McMurry 1988).

2.2. Theoretical

The mobility diameter growth factor g measured by the hygroscopic TnDMA is defined as (Biskos et al. 2006c):

$$g(RH) = \frac{d_m(RH)}{d_{m,dry}}, \quad [1]$$

where $d_{m,dry}$ and $d_m(RH)$ are the mobility diameters of the particles at the dry state (i.e., selected by DMA-1 at <5% RH) and at elevated RH, respectively.

The measured growth factors are compared with predictions that consider the Kelvin effect and the possible change in particle shape from non-spherical (dry solid particles) to spherical (aqueous-solution droplets). The predicted growth factor can be expressed as follows:

$$g(RH) = \left(\frac{100\rho_s}{w_t \rho_{aq}(w_t)}\right)^{1/3} \chi \frac{C_c(\lambda, d_{ve,dry})}{C_c(\lambda, d_{m,dry})}, \quad [2]$$

where ρ_s and χ are the density and the shape correction factor of the dry particles, w_t and $\rho_{aq}(w_t)$ are the water content (weight percent) and the density of the aqueous-solution droplets, and $d_{ve,dry}$ is the volume equivalent diameter of the dry particles. C_c in Equation (2) is the Cunningham slip correction factor given by:

$$C_c(\lambda, d) = 1 + \frac{\lambda}{d}\left[2.34 + 1.05\exp\left(-0.39\frac{d}{\lambda}\right)\right], \quad [3]$$

where λ is the mean free path of the carrier gas, and d the diameter of the particles. Using Equations (2)—(7) we predict the hygroscopic growth of the particles, which can then be compared with the measurements (i.e., Equation (1)).

The particle water content is related to RH through the water activity a_w. For particles having diameters larger than 100 nm, RH = 100 a_w. Particles in the nano-size regime are affected by the curvature and thus by the surface tension of the droplets. The dependence of the water activity to the RH of the particles in this case is given by:

$$RH = 100\ a_w \exp\left(\frac{4M_w\sigma_{aq}(w_t)}{RT\rho_w d_{ve}(RH)}\right), \quad [4]$$

where ρ_w and M_w are the density and molar mass of water, R is the universal gas constant, and T is the temperature. σ_{aq} is the surface tension of the aqueous droplet

given by:

$$\sigma_{aq} = (a + b \times m) \times 10^{-3}. \quad [5]$$

Here m is molality, whereas a and b are material-specific parameters the values of which for the compounds used in this study are given in Table 1. The water content w_t is related to the water activity of the system as follows:

$$a_w = C_i + \sum C_i w_t^i. \quad [6]$$

The polynomial constants in Equation (6) for all salts investigated in this study are provided in Table 1. The density of the aqueous-solution droplets in Equation (2) can be predicted by the polynomial:

$$\rho_{aq} = A_0 + \sum A_i w_t^i, \quad [7]$$

where A_0 and A_i are constants (cf. Table 1 and associated references).

3. Results and discussion

Figure 1 shows the measured and predicted hygroscopic growth curves of KBr nanoparticles during deliquescence- and efflorescence-mode experiments. Deliquescence of the largest particles ($d_{m,dry}$ = 60 nm) occurs between 72.4 and 78.1% RH, whereas efflorescence occurs between 55.3 and 56.2% RH (Table 2). The DRH and ERH values are estimated as the middle point of these ranges, i.e., 75.3 and 55.8%, respectively, which are within ±3% agreement with observations made for large particles and bulk KBr reported in the literature (Martin 2000). Both the DRH and ERH mean values increase monotonically (from 75.3 to 89.7% and from 55.5 to 63.6% RH, respectively) as particle diameter decreases (Figure 1 and Table 2). Best fits of the DRH and ERH as a function of dry particle diameter for the range 8 to 60 nm are $DRH(d_m) = 111.30 d_m^{-0.97} + 75.30$ and $ERH(d_m) = 74.94 d_m^{-0.89} + 55.50$. The particle size distributions measured by DMA-2 when the RH was around the DRH and ERH can exhibit either two narrow distinct peaks (one corresponding to the solid particle state and the other to the aqueous particle state, with the latter including particles that have grown substantially from their dry/solid counterparts), or a broadened peak that includes particle populations in the two different states, with the aqueous particles growing marginally compared to those in the solid state (Figures S1–S4). For the 60-nm KBr particles in the deliquescence-mode experiments, for instance, the recorded mobility distributions are almost identical (i.e., they have the same mean and standard deviation) when the particles are exposed to RH conditions ranging from ca. 8 to 70%. When the RH increases further, the size distributions are slightly shifted to larger particle diameters and become broader. In the efflorescence-mode experiments, on the other hand, the mobility distribution scans for the 60-nm KBr particles are bimodal when the RH is between 56 and 58%, i.e., near the ERH (Figure S1). For RH values higher than the ERH, the mobility distributions of the monodisperse particles are unimodal, albeit broadened, as discussed above. The observation of bimodal distributions can be attributed to inhomogeneities along the experimental setup. Such inhomogeneities can be caused by small differences in the temperature (ca. ±0.5°C during all measurements), and consequently the RH, within the Nafion tube humidity exchanger and DMA-2, causing some of the particles to experience slightly different RH conditions compared to the rest (Bezantakos et al. 2016).

Table 1. Density of the dry particles ρ_s(kg m^{-3}), as well as density of droplet ρ_{aq}(kg m^{-3}), water activity a_w and surface tension σ_{aq}(N m^{-1}) of the solution droplets.

Salt	Density of the dry particles $\rho_s(kg\ m^{-3})$	Density of droplet $\rho_{aq}(Kg\ m^{-3})$ [Forsythe 2003]	Water activity a_w [Robison and Stokes 2002]	Surface Tension $\sigma_{aq}(N\ m^{-1})$
KBr	2750 [Perry and Green 1997]	$A_0 = 1000$ $A_1 = 6.7054$ $A_2 = 0.0597$ $A_3 = -1.0559 \times 10^{-4}$ $A_4 = 2.7455 \times 10^{-6}$	$C_0 = 0.9999$ $C_1 = -0.0027$ $C_2 = -2.2336 \times 10^{-5}$ $C_3 = -4.6610 \times 10^{-7}$ $C_4 = -5.3239 \times 10^{-9}$	$a = 68.573$ $b = 3.7522$ [Shah et al. 2013]
KCl	1987 [Hutchison 1944]	$A_0 = 995$ $A_1 = 7.5$ $A_2 = -8.0 \times 10^{-2}$ $A_3 = 2.667 \times 10^{-3}$	$C_0 = 0.9999$ $C_1 = -0.0043$ $C_2 = -2.5015 \times 10^{-5}$ $C_3 = -1.5253 \times 10^{-6}$ $C_4 = 4.2756 \times 10^{-9}$	$a = 104$ $b = 11.714$ [Shah et al. 2013]
KI	3130 [Perry and Green 1997]	$A_0 = 1001.1$ $A_1 = 6.5929$ $A_2 = 0.0898$ $A_3 = -8.0703 \times 10^{-4}$ $A_4 = 1.438 \times 10^{-5}$	$C_0 = 0.9999$ $C_1 = -0.0020$ $C_2 = -1.5577 \times 10^{-5}$ $C_3 = -4.1034 \times 10^{-7}$ $C_4 = -2.5447 \times 10^{-9}$	$a = 72.792$ $b = 1.1074$ [Ali et al. 2009]

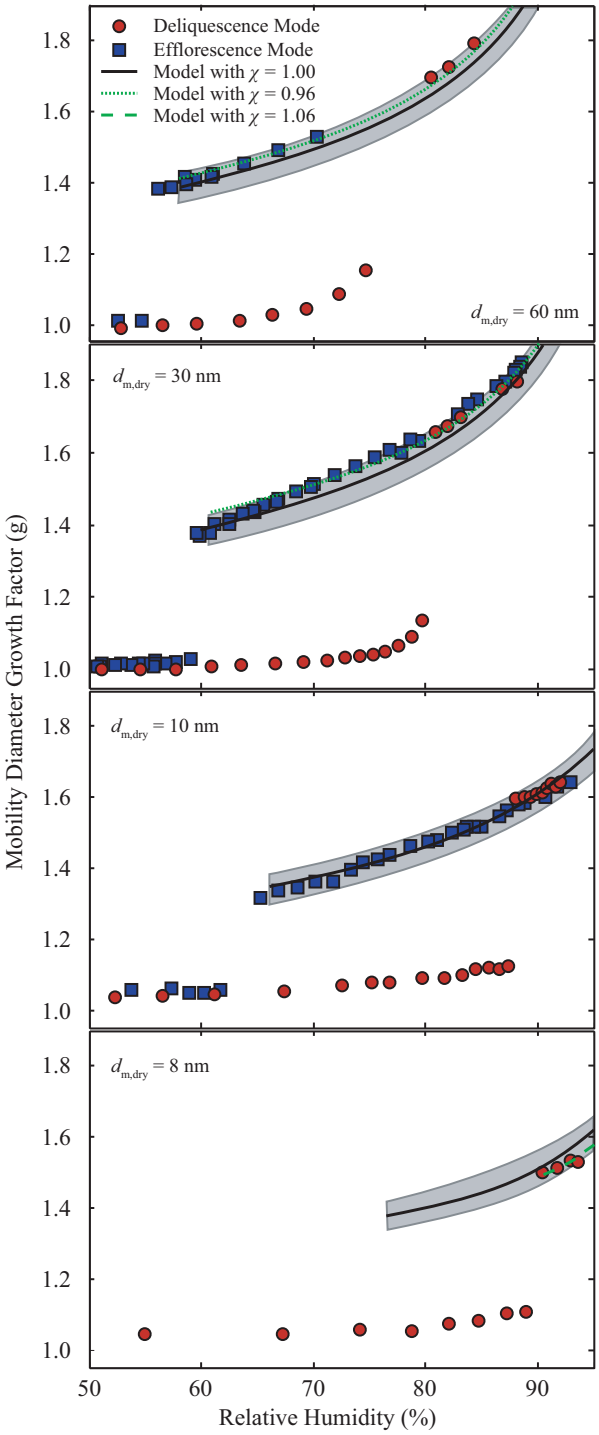

Figure 1. Mobility-diameter growth factors of KBr nanoparticles. Experimental growth factors are shown by the data points: circles correspond to measurements recorded during deliquescence-mode experiments, and squares during efflorescence-mode experiments. In both cases the particles were generated by the vaporization-condensation technique. Lines show the growth factors of the theoretical model, including the Kelvin effect and a shape correction factor. Models are evaluated for $10 < w_t < 80\%$.

The residence time of the particles in the humidifier is significantly longer (of the order of 1.2 s) compared to the time needed for the phase transition (of the order of a few ns; Raoux et al. 2007). Given that the composition of the particles is also uniform, any observed bimodal growth factor distributions can only be explained by RH inhomogeneities in the system (Hameri et al. 2000; Russel and Ming 2002; Tang et al. 1986). Similar behavior was observed for the smaller KBr particles investigated in our study, with bimodal distributions being more often observed as the particle diameter decreased, especially in the efflorescence-mode measurements (Figures S2-S4).

The hygroscopic growth factor of KBr nanoparticles at 75% RH decreases from 1.57 to 1.43 as particle diameter reduces from 60 to 10 nm. For the largest particles investigated here (i.e., 60 and 30 nm in diameter), their dry diameter does not change with increasing RH up to ca. 65%. The small particle growth observed at RH values between ca. 65% and the DRH can be attributed to adsorption of water onto the surfaces of the crystalline particles. As particle size decreases, the apparent growth due to water adsorption is observed at even lower RH values (i.e., ca. 50%) due to the ability of the TnDMA to resolve particle growth corresponding to even one monolayer of adsorbed water in that range. Similar observations are reported for $(NH_4)_2SO_4$ and for NaCl particles in other works (Hameri et al. 2000; Finlayson-Pitts and Hemminger 2000; Wise et al. 2008; Ghosal and Hemminger 1999).

Agreement between measurements and theoretical prediction of the hygroscopic growth of KBr nanoparticles is within experimental uncertainty. It should be noted here that the experimental uncertainty in sizing particles using DMAs, and therefore of the estimated growth factors by the TnDMA measurements, is of the order of ±3% (Kinney et al. 1991). This uncertainty is illustrated by the shaded areas around the model predictions in Figures 1–3. Uncertainties introduced by the accuracy of the RH sensors (which is ±2.5% as stated above) have only marginal contribution in the agreement between measurements and predictions. For the 60- and 30-nm particles, the theoretical predictions are systematically lower compared to the measurements, requiring a shape factor χ of 0.96 to remove the offset. For the 8-nm particles, on the other hand, the theory slightly over-predicts the observations, requiring a shape factor χ of 1.06 to get a good agreement between prediction and measurements. When these shape-factor corrections are taken into account, the agreement between predictions and measurements is within ±1%. Although this improvement indicates that the solid particles may be slightly non-spherical, and that the shape factor of the dry particles can increase non-linearly with decreasing size, differences of this order can also be attributed to the accuracy of the measurements and uncertainty in the

Table 2. Deliquescence and efflorescence RH values and growth factors at 75% RH of KBr, KCl, and KI nanoparticles.

	KBr					KCl					KI				
	DRH range	DRH mean	ERH range	ERH mean	g (75%)	DRH range	DRH mean	ERH range	ERH mean	g (75%)	DRH range	DRH mean	ERH range	ERH mean	g (75%)
60 nm	72.4-78.1	75.3	55.3 — 56.2	55.8	1.57	—	—	—	—	—	53.6-64.3	59.0	40.6-49.9	45.3	1.53
40 nm	77.5-81.1	79.3	57.9 60.0	59.0	1.56	80.8-82.9	81.9	51.4-60.7	56.1	1.44	—		—		—
30 nm	79.7-80.9	80.3	57.8–59.7	58.8	1.52	—	—	—	—	—	54.6-64.4	59.5	41.9-55.6	48.7	1.46
20 nm	80.7-81.7	81.2	58.0-62.1	60.1	1.54	79.6-85.5	82.6	52.6 – 61.8	57.2	1.33	57.1-63.9	60.5	43.1-57.1	50.1	1.45
15 nm	—		62.6-65.0	63.8	1.36	90.5-91.2	90.8	n.t.o.	n.t.o.	1.25	58.4-64.9	61.7	48.6-63.7	56.1	1.4
10 nm	86.9-89.6	88.3	61.0 – 67.6	64.3	1.43	—	—	—	—	—	—	—	—	—	—
8 nm	89.7-91.1	90.4	—		—	n.t.o.	n.t.o.	—	—	—	n.t.o.	n.t.o.	—	—	—
Bulk	79.9-82.0[a]	81.0	52.0[b]			85 ± 1[c] 84.3[d]		56 ± 1[c] 53.0[d]							

[a]Martin (2000); Cohen et al. (1987).
[b]Martin (2000); Zhang and Chan (2002).
[c]Cohen et al. (1987); Freney et al. (2009).
[d]Tang et al. (1986). n.t.o.: no transition observed.

parameters of the theoretical model (e.g., density, surface tension; Hameri et al. 2000, 2001).

Figure 2 shows measured and predicted hygroscopic growth curves for KCl particles during deliquescence- and efflorescence-mode measurements. The DRH mean values increased from 81.9 to 90.8% as particle size decreased from 40 to 15 nm (Table 2). In this particle size range we observed a gradual increase in the growth factors prior to deliquescence, while the corresponding

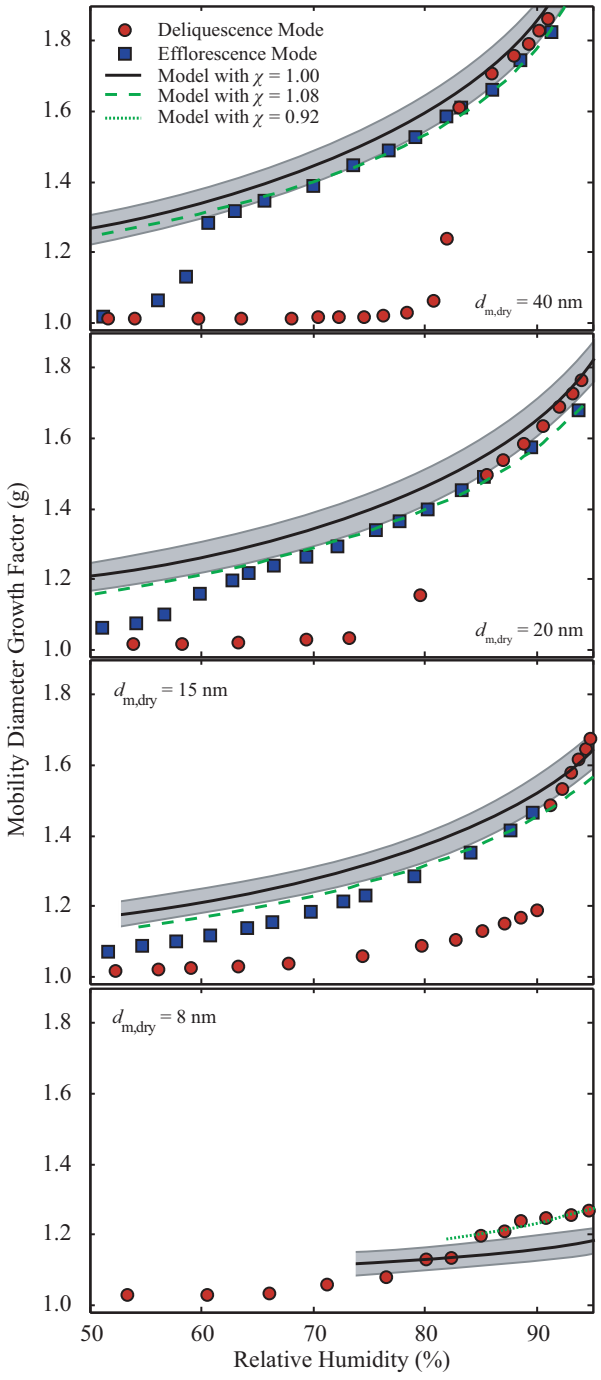

Figure 2. As in Figure 1, but for KCl nanoparticles. Models are evaluated for $10 < w_t < 75\%$.

size distributions were either unimodal and wide or narrower and bimodal (Figures S5-S7). For the 40-nm particles before the DRH point, particle water uptake results in a growth factor of ca. 1.2. The peak of the recorded particle size distributions during the deliquescence-mode experiments (Figure S5) is initially shifted to the right at RH < 80%, becoming bimodal with a smaller peak at ca. 50 nm and a second peak at ca. 60 nm when RH is increased to ca. 81% corresponding to the fully deliquesced particles. At RH > 81% the first peak disappears whereas the second peak gradually shifts to larger particle sizes. Best fits of the DRH and ERH as a function of dry particle diameter for the range 15 to 60 nm are $\mathrm{DRH}(d_m) = 44.36 d_m^{-0.96} + 81.00$.

The mean ERH values of the KCl particles increases from 56.1 to 57.2% as the particle size decreases from 40 to 20 nm (Table 2). At RH values ±15% of the reported mean ERH the measurements show either broad unimodal distributions, or bimodal size distributions having two distinguishable peaks. In both cases, two populations can co-exist in those samples: a population of solid particles and a population of aqueous droplets. As described above, these observations can be attributed to inhomogeneities of the RH in the experimental setup. KCl particles smaller than 20 nm, did not exhibit any apparent efflorescence (cf. Figure S7 in the online supplementary information).

The hygroscopic growth of the KCl particles at 75% RH decreases from 1.47 to 1.21 with decreasing size (Table 2). For particles having sizes ≥15 nm, the theoretical calculations over-predict the observations when not considering any shape correction factor (i.e., $\chi = 1.00$). The over-prediction varies between 2 and 6%, whereas if we use a shape factor correction χ of 1.08 for the dry particles (i.e., corresponding to slightly non-spherical particles) the majority of the data agree with the observations within 3%. It should be noted here that for the 15-nm particles, the slope of the measurements is slightly higher compared to that of the predictions. This, however, can be attributed either to uncertainties in the RH measurements, especially at RH values >95%, or to the difficulty of distinguishing between core-shell particles (KCl crystals coated with water) and fully dissolved droplets due to the small growth factors of the latter at RH values below ca. 70%.

The difficulty to distinguish between crystalline particles coated with water and solution droplets is more evident in the experiments with the 8-nm KCl particles. Here we observed a gradual increase of the growth factor with increasing RH, without a clear phase transition from the solid particle to aqueous-solution droplet. The measured mobility distributions were significantly wider for RH values >55% (Figure S8), indicating the existence

of a second, though not distinguishable, peak. It should be noted that in this size range, water adsorption onto the particles prior deliquescence can cause an increase in particle size of the order of a nanometer, yielding a growth factor in the range of that observed here. Considering also that the growth of the 8-nm KCl particles is not as high as that of the KI particles discussed above, distinguishing between completely deliquesced (i.e., solution droplets) and coated (solid particles with a few adsorbed monolayers of water) with the current system is challenging. By estimating the growth factors using the mean size of the broadened size distributions, the measurements can be fitted by the theoretical model when a shape factor correction of 0.92 is used. Such a correction may suggest that the dry particles are slightly non-spherical but more streamlined compared to the spherical droplets. This interpretation, however, is rather unlikely, and thus the shape factor correction can only provide an estimate of the contribution of other experimental uncertainties associated to these measurements.

The measured and predicted hygroscopic growth curves for the KI nanoparticles are shown in Figure 3. The mean DRH in this case increases from 59.0 to 61.7% (Table 2) as the particle size decreases from 60 to 15 nm. In a similar manner, the ERH mean values increase from 45.3 to 56.1% as particle size decreases in the same range. In a similar manner with the previously described measurements for KBr and the KCl nanoparticles, the size distributions recorded by DMA-2 and the CPC during deliquescence-mode experiments are bimodal just prior deliquescence, while they become unimodal and broader near the DRH point for the other particle diameters studied here (Figure S9–S12). The small diameter increase ($g < 1.1$) prior deliquescence of all particle sizes having diameter $\geq$15 nm can be attributed to water adsorption. During the efflorescence-mode measurements, all the recorded size distributions using KI particles in this size range remain unimodal and become significantly wider near the ERH. Best fits of the DRH and ERH as a function of dry particle diameter for the range 15 to 60 nm are $DRH(d_m) = 4.37 \times 10^4 d_m^{-3.54} + 59$ and $ERH(d_m) = 3879.80 d_m^{-2.18} + 45.30$.

Contrary to the KI particles having diameters larger than 15 nm that exhibit a clear phase transition during deliquescence- and efflorescence-mode experiments, the 8-nm KI particles exhibit a gradual increase of the growth factor over the entire range of RHs, while the associated size distributions remain unimodal with insignificant change of their standard deviation (Figure S12). The lack of any clear phase transition from the solid to the aqueous particles, however, cannot exclude that the particles do not become droplets past a specific RH value. Solution droplets may exist in some of the measurements

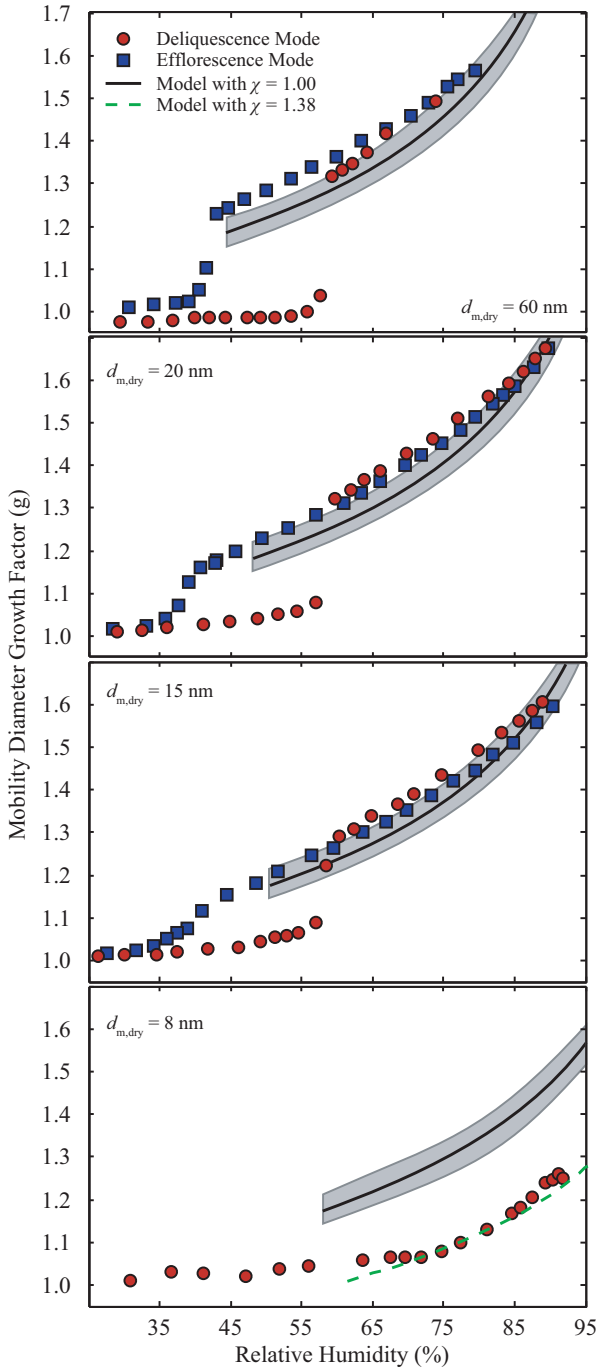

Figure 3. As in Figure 1, but for KI nanoparticles. Models are evaluated for $10 < w_t < 75\%$.

but they may have too small sizes for the TnDMA to distinguish from those of water-coated crystalline particles prior to deliquescence.

The growth factors of the KI nanoparticles at 75% RH decrease from 1.53 to 1.30 as the particle mobility diameter decreases from 60 to 15 nm. Experimental data and theoretical predictions that do not consider any shape correction factor (i.e., $\chi = 1.00$) for particles in this size range agree within ±3% at RH values larger than ca. 75%. The discrepancy between measurements and predictions

is larger at lower RHs, but this can still be explained by uncertainties in the measurements and/or of the parameters used in the theoretical model. The deliquescence-mode measurements with the 8-nm KI particles, on the other hand, deviate significantly from the theoretical predictions. In this case, the theoretical model predictions fit the measurements only when we apply a shape correction factor of 1.38, suggesting that the shape of the dry 8-nm particles is non-spherical. Although this possibility cannot be excluded, it is more likely that the discrepancy between measurements and predictions observed here can be the result of the particles not deliquescing within the RH range investigated here (up to 92%).

4. Conclusions

Measurements of the hygroscopic behavior of three potassium halide salt nanoparticles, namely KBr, KCl and KI, are reported in this article. All salts studied here exhibit a behavior similar to that observed previously for NaCl nanoparticles (Flagan and Lunden 1995; Rader and McMurry 1986). The deliquescence and the efflorescence RH values increase while the associated growth factors decrease as the particle size reduces below 50 nm.

The data for KBr nanoparticles having sizes in the entire range investigated here (i.e., from 8 to 60 nm) showed clearly resolved deliquescence. Deliquescence was also well resolved for KCl and KI nanoparticles for particles having diameters $\geq$15 nm. Efflorescence of those particles was also clearly resolved, although the population of the smaller particles exhibited a simultaneous phase transition compared to their larger counterparts. For KCl and KI particles having diameters of 8 nm, growth factors were sufficiently small that the resulting droplets after deliquescence could not be distinguished from water-coated crystalline particle prior to deliquescence.

The growth factors for all salt nanoparticles investigated in this work decrease progressively as dry particle decreases. With the exception of the 8-nm KI particles, all observations agree, within expected uncertainties, with theoretical predictions. By including corrections that take into account changes of the shape of the particles when these are in the dry crystalline (non-spherical particles having a shape factor $\neq 1$) or the solution droplet (spherical particles having a unity shape factor) phase, agreement between measurements and predictions was further improved.

ORCID

G. Biskos http://orcid.org/0000-0003-0512-6115

References

Ali, K., Shah, A. A., Bilal, S., and Shah, A. A. (2009). Surface tensions and thermodynamic parameters of surface formation of aqueous salt solutions: III. Aqueous solution of KCl, KBr and KI. *Colloids and Surfaces A: Physicochem. Eng. Aspects*, 337:194–199. doi:10.1016/j.colsurfa.2008.12.023.

Anastastio, C., and Martin, S. T. (2001). Atmospheric nanoparticles. *Nanoparticles Environ.*, 44:293–349.

Bezantakos, S., Huang, L., Barmpounis, K., Martin, S. T., and Biskos, G. (2016). Relative humidity non-uniformities in Hygroscopic Tandem Differential Mobility Analyzer measurements. *J. Aerosol Sci.*, 101:1–9. doi:10.1016/j.jaerosci.2016.07.004.

Biskos, G., Malinowski, A., Russel, L. M., Buseck, P. R., and Martin, S. T. (2006a). Nanosize effect on the deliquescence and the efflorescence of sodium chloride particles. *Aerosol Sci. Technol.*, 40:97–106. doi:10.1080/02786820500484396.

Biskos, G., Paulsen, D., Russell, L. M., Buseck, P. R., and Martin, S. T. (2006b). Prompt deliquescence and efflorescence of aerosol nanoparticles. *Atmos. Chem. Phys.*, 6:4633–4642. doi:10.5194/acp-6-4633-2006.

Biskos, G., Russell, L. M., Buseck, P. R., and Martin, S. T. (2006c). Nanosize effect on the hygroscopic growth factor of aerosol particles. *Geophys. Res. Lett.*, 33:L07801. doi:10.1029/2005GL025199.

Cohen, M. D., Flagan, R. C., and Seinfeld, J. H. (1987). Studies of concentrated electrolyte solutions using the electrodynamic balance. 3. Solute nucleation. *J. Phys. Chem.*, 91:4563–4574. doi:10.1021/j100301a029.

Finlayson-Pitts, B. J., and Hemminger, J. C. (2000). Physical chemistry of airborne sea salt particles and their components. *J. Phys. Chem. A*, 104:11463–11477. doi:10.1021/jp002968n.

Flagan, R. C., and Lunden, M. M. (1995). Particle structure control in nanoparticle synthesis from the vapor phase. *Mater. Sci. Eng. A*, 204:113–124. doi:10.1016/0921-5093(95)09947-6.

Forsythe, W. E. (2003). Smithsonian Physical Tables.

Freney, E., Martin, S., and Buseck, P. (2009). Deliquescence and efflorescence of potassium salts relevant to biomass-burning aerosol particles. *Aerosol Sci. Technol.*, 43:799–807. doi:10.1080/02786820902946620.

Gao, Y., Chen, S. B., and Yu, L. E. (2006). Efflorescence relative humidity for ammonium sulfate particles. *J. Phys. Chem. A*, 110:7602–7608. doi:10.1021/jp057574g.

Gao, Y., Chen, S. B., and Yu, L. E. (2007). Efflorescence relative humidity of airborne sodium chloride particles: A theoretical investigation. *Atmos. Environ.*, 41:2019–2023. doi:10.1016/j.atmosenv.2006.12.014.

Ghosal, S., and Hemminger, J. C. (1999). Effect of water on the HNO3 pressure dependence of the reaction between gas-phase HNO3 and NaCl surfaces. *J. Phys. Chem. A*, 103:4777–4781. doi:10.1021/jp991142m.

Hameri, K., Vakeva, M., Hansson, H. C., and Laaksonen, A. (2000). Hygroscopic growth of ultrafine ammonium sulphate aerosol measured using an ultrafine tandem differential mobility analyzer. *J. Geophys. Res.*, 105:22231–22242. doi:10.1029/2000JD900220.

Hameri, K., Laaksonen, A., Vakeva, M., and Suni, T. (2001). Hygroscopic growth of ultrafine sodium chloride particles. *J. Geophys. Res.*, 106:20749–20757. doi:10.1029/2000JD000200.

Hutchison, D. A. (1944). Density of Potassium Chloride. *Physical Review*, 66:144–148. doi:10.1103/PhysRev.66.144.

Kelly, J. T., and Wexler, A. S. (2006). Water uptake by aerosol: Water activity in supersaturated potassium solutions and deliquescence as a function of temperature. *Atmos. Environ.*, 40:4450–4468. doi:10.1016/j.atmosenv.2006.04.017.

Kinney, P. D., Pui, D. Y. H., Mulholland, G. W., and Bryner, N. P. (1991). Use of the electrostatic classification method to 0.1 μm SRM particles -A Feasibility Study. *J. Res. Natl. Inst. Stand. Technol.*, 96:147. doi:10.6028/jres.096.006.

Köhler, H. (1936). The nucleus in and the growth of hygroscopic droplets. *Trans. Faraday Soc.*, 32:1152–1161. doi:10.1039/TF9363201152.

Liu, X. D., Van Espen, P., Adams, F., Cafmeyer, J., and Maenhaut, W. (2000). Biomass burning in southern Africa: Individual particle characterization of atmospheric aerosols and savanna fire samples in southern Africa. *J. Atmos. Chem.*, 36:135–155. doi:10.1023/A:1006387031927.

Markwardt, C. (2010). MPFIT: A MINPACK-1 Least Squares Fitting Library in C, at http://www.physics.wisc.edu/~craigm/idl/cmpfit.html.

Marquardt, D. W. (1963). An algorithm for least-squares estimation of nonlinear parameters. *SIAM*, 11:431–441.

Martin, S. T. (2000). Phase transitions of aqueous atmospheric particles. *Chem. Rev.*, 100:3403–3453. doi:10.1021/cr990034t.

Mifflin, A. L., Smith, M. L., and Martin, S. T. (2009). Morphology hypothesized to influence aerosol particle deliquescence. *Phys. Chem. Chem. Phys.*, 11:10095–10107. doi:10.1039/b910432a.

Perry, H. R., and Green, W. D. (1997). *Perry's Chemical Engineers' Handbook*. McGraw-Hill, United States.

Pruppacher, H. R., and Klett, J. D. (1997). Microphysics of clouds and precipitation, Kluwer.

Rader, D. J., and McMurry, P. H. (1986). Application of the tandem differential mobility analyzer to studies of droplet growth or evaporation. *J. Aerosol Sci.*, 17:771–787. doi:10.1016/0021-8502(86)90031-5.

Raoux, S., et al. (2007). Direct observation of amorphous to crystalline phase transitions in nanoparticle arrays of phase change materials. *J Applied Physics*, 102:094305. doi:10.1063/1.2801000.

Robinson, R. A., and Stokes, R. H. (2002). *Electrolyte solutions*. Dover Publications Inc., United States.

Russell, L. M., and Ming, Y. (2002). Deliquescence of small particles. *J. Chem. Phys.*, 116:311–321. doi:10.1063/1.1420727.

Scheibel, H. G., and Porstendörfer, J. (1983). Generation of monodisperse Ag and NaCl aerosols with particle diameters between 2 and 300nm. *J. Aerosol Sci.*, 14:113–126. doi:10.1016/0021-8502(83)90035-6.

Seinfeld, J. H., and Pandis, S. N., (2006). *Atmospheric chemistry and physics: From air pollution to climate change*. Wiley, United States.

Shah, A. A., Ali, K., and Bilal, S. (2013). Surface tension, surface excess concentration, enthalpy and entropy of surface formation of aqueous salt solutions. *Colloids and Surfaces A: Physicochem. Eng. Aspects*, 414:183–190. doi:10.1016/j.colsurfa.2012.10.054.

Stolzenburg, M. R., and McMurry, P. H., (1988). *TDMAFIT users manual*. University of Minnesota, Department of Mechanical Engineering, Particle Technology Laboratory, United States.

Tang, I. N., and Munkelwitz, H. R. (1977). Aerosol growth studies—III ammonium bisulfate aerosols in a moist atmosphere. *J. Aerosol Sci.*, 8:321–330. doi:10.1016/0021-8502(77)90019-2.

Tang, I. N., Munkelwitz, H. R., and Wang, N. (1986). Water activity measurements with single suspended droplets: The NaCl-H2O and KCl-H2O systems. *J. Colloid Interf. Sci.*, 114:409–415 doi:10.1016/0021-9797(86)90426-1.

Tang, I. N., and Munkelwitz, H. R. (1993). Composition and temperature dependence of the deliquescence properties of hygroscopic aerosols. *Atmos. Environ.*, 8:467–473. doi:10.1016/0960-1686(93)90204-C.

Tang, I. N., and Munkelwitz, H. R. (1994). Aerosol phase transformation and growth in the atmosphere. *J. Appl. Meteorol.*, 33:791–796. doi:10.1175/1520-0450(1994)033<0791:APTAGI>2.0.CO;2.

Tang, I. N. (1996). Chemical and size effects of hygroscopic aerosols on light scattering coefficients. *J. Geophys. Res.*, 101:19245–19250. doi:10.1029/96JD03003.

Tang, I. N., Tridico, A. C., and Fung, K. H. (1997). Thermodynamic and optical properties of sea salt aerosols. *J. Geophys. Res.*, 102:23269–23275. doi:10.1029/97JD01806.

Topping, D. (2008). Thermodynamics of Aqueous Systems In: *Environomental chemistry of aerosols*. Blackwell Publishing Ltd, United Kingdom, pp. 141–191.

Wexler, A. S., and Seinfeld, J. H. (1991). Second-generation inorganic aerosol model. *Atmos. Environ.*, 25A:2731–2748. doi:10.1016/0960-1686(91)90203-J.

Wise, M. E., Biskos,G., Martin, S. T., Russell, L. M., and Buseck, P. R. (2005). Phase transitions of single salt particles studied using a transmission electron microscope with an environmental cell. *Aerosol Sci. Technol.*, 39:849–856. doi:10.1080/02786820500295263.

Wise, M. E., Martin, S. T., Russel, L. M., and Buseck, P. R. (2008). Water uptake by NaCl particles prior to deliquescence and the phase rule. *Aerosol Sci. Technol.*, 42:281–294. doi:10.1080/02786820802047115.

Zhang, Y. H., and Chan, C. K. (2002). Understanding the hygroscopic properties of supersaturated droplets of metal and ammonium sulfate solutions using Raman spectroscopy. *J. Phys. Chem. A*, 106:285–292. doi:10.1021/jp012694j.